Metallo-inhibition of Mnx, a bacterial manganese multicopper oxidase complex

Alexandra V. Soldatova,[†] Wen Fu,[#] Christine A. Romano,[§,⊥] Lizhi Tao,[#] William H. Casey,[#,⊥] R. David Britt,[#] Bradley M. Tebo,[§] and Thomas G. Spiro*,[†]

[†]Department of Chemistry, University of Washington, Box 351700, Seattle, Washington 98195, United States

[§]Division of Environmental and Biomolecular Systems, Institute of Environmental Health, Oregon Health & Science University, Portland, Oregon 97239, United States

[#] Department of Chemistry and [⊥]Earth and Planetary Sciences Department, University of California, Davis, One Shields Avenue, Davis, California 95616, United States

[⊥]Present Address: Metagenomi, 1545 Park Ave, Emeryville, California, 94608

*Corresponding Author: spiro@chem.washington.edu

ABSTRACT

The manganese oxidase complex, Mnx, from *Bacillus* sp. PL-12 contains a multicopper oxidase (MCO) and oxidizes dissolved Mn(II) to form insoluble manganese oxide (MnO_2) mineral. Previous kinetic and spectroscopic analyses have shown that the enzyme's mechanism proceeds through an activation step that facilitates formation of a series of binuclear Mn complexes in the oxidation states II, III, and IV on the path to MnO_2 formation. We now demonstrate that the enzyme is inhibited by first-row transition metals in the order of the Irving-Williams series. Zn(II) strongly ($K_i \sim 1.5$ μM) inhibits both activation and turnover steps, as well as the rate of Mn(II) binding. The combined Zn(II) and Mn(II) concentration dependence establishes that the inhibition is non-competitive. This result is supported by electron paramagnetic resonance (EPR) spectroscopy, which reveals unaltered Mnx-bound Mn(II) EPR signals, both mono- and binuclear, in the presence of Zn(II). We infer that inhibitory metals bind at a site separate from the substrate sites and block the conformation change required to activate the enzyme, a case of allosteric inhibition. The likely biological role of this inhibitory site is discussed in the context of *Bacillus* spore physiology. While Cu(II) inhibits Mnx strongly, in accord with the Irving-Williams series, it increases Mnx activation at low concentrations, suggesting that weakly bound Cu, in addition to the four canonical MCO-Cu, may support enzyme activity, perhaps as an electron transfer agent.

1. INTRODUCTION

Manganese biomineralization by manganese-oxidizing microorganisms is the dominant route of manganese oxide deposition on Earth, and a key pathway of the global Mn cycle. Some bacteria and fungi oxidize Mn(II) indirectly, first producing superoxide radical (O_2^-), which then oxidizes Mn(II) to Mn(III), later forming MnO_2 mineral [1-5]. However, many other microorganisms have evolved the ability to catalyze direct oxidation of Mn(II), producing nanoparticulate MnO_2 that subsequently condenses to form MnO_2 minerals [6]. Enzymatic manganese biomineralization is widespread, occurring in terrestrial, freshwater, and marine environments [7, 8]. It has been found that some bacteria use peroxides to oxidize Mn(II), catalyzed by calcium-binding animal heme peroxidases [9, 10] (specifically by enzymes from the cyclooxygenase-peroxidase superfamily [5, 11]), but many other phylogenetically diverse Mn-oxidizing organisms utilize O_2 directly via multicopper oxidases (MCO) [12-17]. The MCO enzyme family relies on at least 4 copper cofactors to couple oxidation of a wide variety of substrates, both organic and inorganic, at a type 1 copper center (T1-Cu) with reduction of O_2 to water at a trinuclear copper center [18, 19]. Numerous attempts to purify an active Mn-oxidizing MCO enzyme were unsuccessful until 2012 [20], when the Tebo lab succeeded in heterologously producing an active manganese oxidase Mnx, from *Bacillus* sp. PL-12, a halotolerant organism isolated from marine sediments [21], but closely related to species from soil environments. Mnx is a complex of MnxG, a large (138 kDa) multicopper oxidase, tightly bound to three copies each of small (12 kDa) accessory proteins, MnxE and MnxF [20, 22]. While MnxE and MnxF do not have close homologues, MnxG was found to be similar to the human ferroxidase ceruloplasmin. However, unlike ceruloplasmin, MnxG catalyzes two successive and energetically difficult one-

electron oxidation steps, and produces MnO_2 biomineral as a final product, representing a new subclass of Mn(II)-mineralizing MCO enzymes.

Detailed spectroscopic and kinetic measurements [23, 24] led us to propose the mechanism for Mn(II) oxidation shown in Fig. 1.
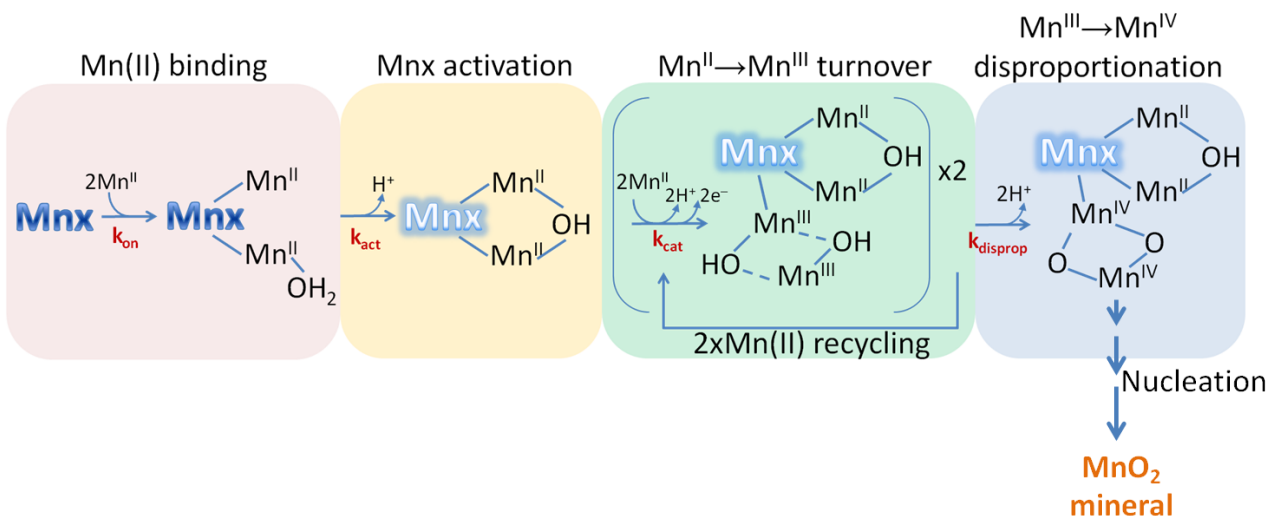
Fig. 1. Proposed Mnx mechanism of Mn(II) oxidation and MnO_2 formation: Two Mn(II) bind at the Mnx substrate site (Mn(II) binding step), and form a hydroxide-bridged activated complex, [Mn(II),Mn(II)](OH), following a protein conformation change and Mn(II)-OH_2 deprotonation (Mnx activation step). Electron transfer and Mn(III) translocation leaves [Mn(II),Mn(III)](OH), and turnover produces a dihydroxide-bridged Mn(III) intermediate, [Mn(III),Mn(III)]$(OH)_2$ ($Mn^{II} \rightarrow Mn^{III}$ turnover step). Two of these intermediates subsequently disproportionate to two Mn(II) ions, which are recycled, and a dioxo-bridged Mn(IV) product, [Mn(IV),Mn(IV)]$(O)_2$ ($Mn^{III} \rightarrow Mn^{IV}$ disproportionation step), which then condenses into MnO_2 nanoparticles (nucleation step).

Two Mn(II) ions bind to Mnx and induce a conformation change that brings the two Mn(II) together via a hydroxide bridge, following deprotonation of Mn(II)-bound H_2O [23]. The Mn(III)/Mn(II) reduction potential is thereby lowered sufficiently to permit oxidation by the T1-Cu, producing a doubly hydroxide-bridged binuclear Mn(III) intermediate. This intermediate disproportionates to oxo-bridged Mn(IV) and Mn(II), which recycles back to the Mn(II) substrate site. The oxo-bridged Mn(IV) then condenses to form MnO_2 nanoparticles [24].

In the environment, further transformation and abiotic partial reduction of the resulting biogenic MnO_2 nanoparticulate product leads to a variety of Mn(III,IV) oxides [25-32]—highly reactive mineral phases that are capable of scavenging and oxidizing not only organics, but also many trace metals, including toxic metals [33-38]. Indeed, numerous studies have explored how incubation of Mn-oxidizing bacteria with different metals affects the structure and composition of the biogenic manganese oxides product [29, 39-47], and technologies are being pursued to use bacterially produced manganese oxide to clean contaminated waters [34, 48-54]. However, how the presence of other metals interferes with the enzymatic mechanism of Mn oxidation remained unknown in the absence of a purified enzyme from an Mn-oxidizing organism. Each step of the proposed Mnx enzymatic mechanism in Fig. 1 can potentially be influenced by other metals. Studies with whole cells have demonstrated that different metals can get incorporated into the MnO_2 [29, 39, 40, 44, 45, 55], presumably by affecting condensation of the primary enzymatic product into the mineral structure. However, other metals could also bind directly to the enzyme, competing with Mn(II) for Mnx binding sites, or interfering with the Mn(II) oxidation by disrupting formation of hydroxo- and oxo-bridges, or slowing down the enzyme conformation change. In this study, we address the question of how first-row transition metals affect Mn(II) oxidation by Mnx. Zn(II) powerfully inhibits all stages of Mnx catalysis, and does so non-competitively, a conclusion supported by EPR spectroscopy, which shows that Zn(II) has no effect on the Mnx-bound Mn(II) signals. Thus, Zn(II) binds at an inhibitory site, separate from the substrate site. Other divalent metals inhibit the reaction according to the Irving-Williams order (Co(II) < Ni(II) < Cu(II) > Zn(II) [56, 57]). Cu(II), however, stimulates the enzyme at low concentrations, playing an additional role in catalysis. We propose a mechanism accounting for

inhibition and offer hypotheses on the role of Zn(II) inhibition in the physiology of Mn-oxidizing *Bacillus* spores.

2. METHODS

2.1. Spectroscopic Measurements

Manganese-oxidation assays were monitored via the growth of a ligand-to-metal charge-transfer absorption band of the MnO_2 enzymatic product, using an Agilent 8453 UV–vis spectrophotometer (Santa Clara, CA, USA) with a multicell configuration and automated kinetic scan capability, in 10 mm pathlength cuvettes. The samples were stirred continuously with a Spinette magnetic stirrer (Starna Cells, Atascadero, CA, USA). For reactions taking longer than an hour, several assays were monitored in a parallel configuration. For faster reactions, one assay was monitored at a time.

2.2. Reaction assays

Mnx expression and purification has been described previously [58]. All metal dependences described in this study were obtained from a single Mnx stock, to avoid any variations in activity that can be expected from different batches of protein expression and purification. Oxidation assays (1 mL total volume) contained 50 nM Mnx in 10 mM HEPES buffer, pH 7.8. Mnx stock with an added aliquot of inhibiting metal was equilibrated for 5–10 min in the spectrophotometer cuvette. Then, Mn-oxidation was initiated by adding an aliquot of 0.01 M $MnSO_4$ stock to the cuvette. The cuvette was capped, inverted several times to ensure complete mixing, and returned to the spectrophotometer for measurements. The time for substrate addition and mixing, ~12 s, set time zero for the time course. A series of Zn(II)-inhibition experiments was performed, at three different starting Mn(II)-concentrations: 20 μM, 50 μM, and 100 μM, and varying Zn(II) concentrations, from 0.2 μM to 25 μM (added as $ZnSO_4$). Inhibition experiments with Co(II)

(added as $CoCl_2$), Ni(II) (added as $NiCl_2$), and Cu(II) (added as $CuSO_4$) were performed at a single Mn(II) concentration of 50 μM. All metal salts had a purity of 99% or more; contamination from other metals was insignificant. Previously we described the sensitivity of Mnx assays to UV light (even from the spectrophotometer UV source), enhanced by the presence of the HEPES buffer [23]. Consequently, the kinetic data acquisition was performed under the visible lamp only to prevent unwanted reductive reactions by HEPES under UV light, and spectral evolution was monitored in the 340–900 nm region (Fig. S1).

2.3. Data analysis

The evolving spectra were corrected for a small scattering background at longer wavelengths that developed as the reaction progressed. The spectra showed growth of the MnO_2 absorption band, accompanied by a red-shift, which we separated by applying multivariate analysis, using the MCR-ALS (Multivariate Curve Resolution–Alternating Least-Squares) algorithm developed and implemented as a graphical interface by Tauler et al. [59-61] and run in the MATLAB 8.3 environment (The MathWorks, Inc.), as described before [23]. The spectral changes could be represented by just two components, corresponding to the initial enzyme product (S1 component), and the mature MnO_2 nanoparticles (S2 component). Because the reaction ran to completion, the spectral absorbance at the end of each experimental run provided the molar extinction coefficient. However, this coefficient is unknown for the early spectra corresponding to initial enzymatic product, and was scaled to 80% of the final coefficient, based on our report of the size-dependent absorption properties of synthetic MnO_2 preparations [62]. Further comparison of the spectra of final MnO_2 produced at higher concentrations of metal inhibitors (Fig. S2) revealed that the absorption strength of the MnO_2 band is variable. To eliminate any uncertainties in normalization during the MCR procedures, all final concentrations of the S1

6

enzymatic components were normalized to reach the expected Mn concentrations (i.e. 20, 50, or 100 μM).

2.4. EPR Spectroscopy

X-band (9.38 GHz) continuous-wave (CW) EPR spectra were recorded on a Bruker (Billerica, MA) EleXsys E500 spectrometer equipped with a super-high Q resonator (ER4122SHQE). Cryogenic temperatures were achieved and controlled using an ESR900 liquid helium cryostat in conjunction with a temperature controller (Oxford Instruments ITC503) and gas flow controller. CW EPR data were collected under slow-passage, non-saturating conditions at 15 K. The spectrometer settings were as follows: conversion time = 40 ms, field modulation frequency = 100 kHz, and field modulation amplitude = 0.8 mT.

3. RESULTS

3.1. Newly expressed protein confirms the previous kinetic scheme and parameters

The Mnx complex was first expressed and purified using the *mnxDEFG* expression construct from *Bacillus* sp. PL-12, but only the *mnxEFG* operon gene products were detected in the active enzyme complex [20]. Subsequent characterization showed that the active Mnx complex consists of one subunit of the multicopper oxidase MnxG (138 kDa) and six subunits of the smaller accessory proteins (12 kDa) MnxE and MnxF, assembled as an alternating ring [22]. The significance of the highly conserved *mnxD* gene among different Mn-oxidizing *Bacillus* species is not known, but this small (~30 kDa) gene product is not present in the Mnx complex. Omitting the *mnxD* gene in the expression system does not affect the yield and Mn-oxidizing ability of the Mnx enzyme [58]. In this work, we employed a plasmid with the gene construct of *mnxEFG* to express and purify Mnx, and verified the previously characterized oxidation mechanism [23]. As before, the production of colloidal MnO_2 was monitored via its ~350 nm absorption band, after

varying amounts of MnSO$_4$ were added to 50 nM Mnx in HEPES buffer. The enzyme reaction was distinguished from subsequent maturing of the MnO$_2$ product (red-shifted absorption) using the MCR-ALS chemometric procedure. The enzymatic traces are sigmoidal, a slow induction phase being followed by linear growth. They were fit (Fig. S3) with the activation equation [63]:

$$[MnO_2] = V_{s-s} * (x - x_0) - \frac{V_{s-s}}{k_{act}} * (1 - e^{-k_{act}*(x-x_0)}) \quad (1)$$

to extract k_{act}, the rate constant for enzyme activation, V_{s-s}, the subsequent steady-state velocity, and x_0, the lag before reaction starts. The Mn(II) concentration dependences of the kinetic parameters (Fig. S4) are similar to those previously reported [23]. Thus, the mechanism of Mn(II) oxidation does not depend on whether *mnxEFGD* or *mnxEFG* gene constructs are used to express the Mnx complex.

*3.2. Inhibition of Mnx reaction by Zn(II)*

In view of numerous observations that divalent metals inhibit the manganese oxidizing activity of spore extracts and whole bacteria [39, 40, 64-69], we thought to investigate the enzymatic mechanism behind this inhibition. MnO$_2$ production by Mnx was noticeably slowed by quite low (0.2 μM) concentrations of Zn(II), although the growth of the MnO$_2$ absorption band remained sigmoidal as the Zn(II) concentration increased (Fig. 2).
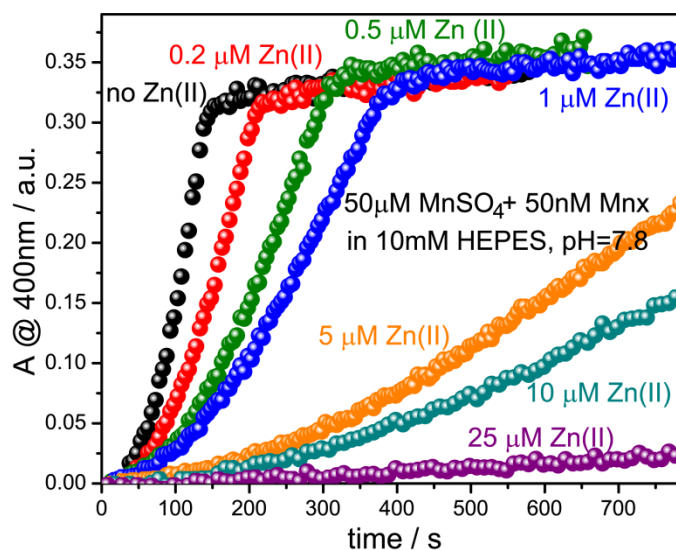
Fig. 2. Progress curves taken at 400 nm during Mnx-catalyzed oxidation of 50 μM MnSO₄ in the presence of indicated concentrations of Zn(II), in 10 mM HEPES, pH 7.8.

3.2.1. EPR shows that Zn(II) does not compete with Mn(II) binding

We tested the hypothesis that inhibition is due to Zn(II) competition for the Mn(II) binding sites on Mnx (similar to Zn(II) inhibition of Fe(II) oxidation in MCOs ceruloplasmin [70] and Fet3p [71]) using EPR spectroscopy. Mnx-bound mononuclear and dinuclear Mn(II) EPR signals (designated as "class ii" and "class iii", respectively, in [72]) were previously detected when Mn(II) is added to Mnx [72], the mixture likely reflecting weaker Mn(II) binding to a second site. These signals should be suppressed if Zn(II) binds competitively with Mn(II), but addition of Zn(II) had no effect on either signal, even after oxygen was added to the mixture to initiate the reaction (Fig. 3). Thus, the EPR evidence strongly indicates noncompetitive binding of Zn(II) inhibitor.
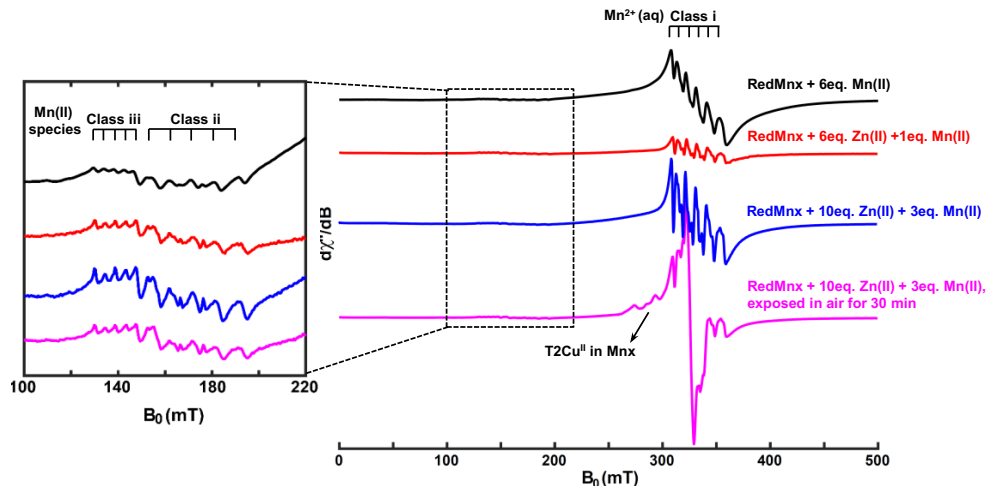
Fig. 3. X-band CW EPR spectra of the Mnx protein complex that was anaerobically reduced with dithionite, with the excess dithionite removed by a desalting column. The reduced Mnx (redMnx) was then anaerobically incubated with 6 or 10 equivalent of Zn(II) before the addition of indicated amount of Mn(II) substrate.

3.2.2. Lag phase and activation kinetics both establish noncompetitive inhibition

Zn(II) inhibition was analyzed through a series of kinetic assays at three Mn(II) concentrations: 20 μM, 50 μM, and 100 μM, and varying Zn(II) concentrations from 0.2 μM to 25 μM. The enzymatic traces, extracted from time-resolved spectral data using the MCR-ALS analysis, were fit with the activation equation (1), which remains valid for reactions taking place in the presence of inhibitor, although the enzyme activation rate constant, k_{act}, becomes a complex function of inhibitor concentration (equation (12) in ref. [63]). The obtained lag phase, activation rate constant, and turnover rate parameters (Fig. S5–S7) were used for subsequent analysis below.

The lag phase, which corresponds to slow initial Mn(II) binding to Mnx, increases linearly with increasing Zn(II) concentration (Fig. 4A), but the degree of Zn(II) inhibition scales inversely with Mn(II) concentration. The enzyme activation step that follows Mn(II) binding is also inhibited by the presence of Zn(II): k_{act} decreases rapidly with Zn(II), before it disappears completely at [Zn(II)] > 10 μM, with no apparent dependence on Mn(II) concentration (Fig. 4B).

10

(For 20 µM Mn(II) the trend is uncertain with Zn(II) added up to 1 µM, and the activation step disappears when Zn(II) concentration increases beyond 5 µM (Fig. S5).)
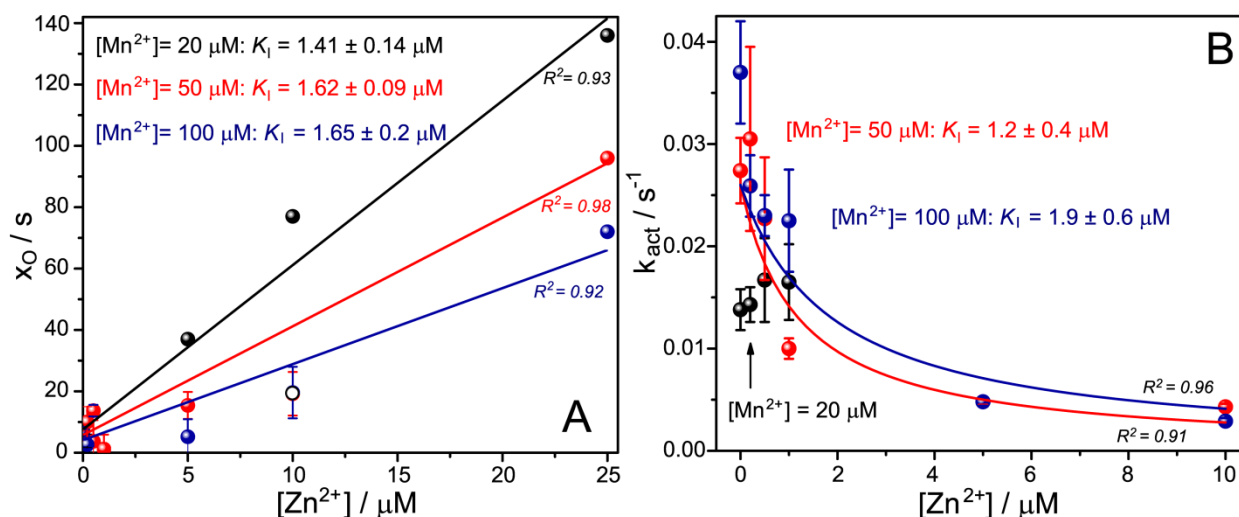
Fig. 4. Inhibition of Mn(II) binding step, expressed as a lag phase x_o (A), and of Mnx activation step k_{act} (B) by Zn(II) during Mnx-catalyzed oxidation of indicated amount of $MnSO_4$ in 10 mM HEPES buffer, pH 7.8. The lag phase dependences were fit to equation (2) (open points—an assay error in the 10 µM runs—were excluded from the fit); the activation rate constant dependences were fit to equation (3).

To account for the observed x_o and k_{act} dependences on Zn(II), a general mechanism of an activatable enzyme in the presence of an inhibitor can be invoked [63]:
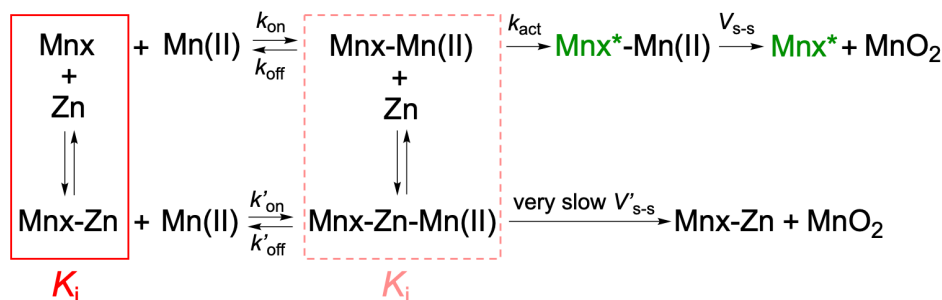
In our case we assume that (1) conversion to the active Mnx conformation (Mnx* in green in the scheme above) is triggered by substrate binding only; (2) Zn(II) binding to activated Mnx is negligible; (3) binding of Zn(II) to Mnx is unaffected by the presence of Mn(II) (red

11

boxes in the scheme above); and (4) Zn-bound Mnx is not activated by Mn(II) so that the activation rate constant in the presence of Zn(II) approaches zero ($k'_{act} \rightarrow 0$) with increasing Zn.

When Mn(II) is added to the Mnx assay that had been pre-equilibrated with Zn(II), the enzyme exists in an equilibrium Mnx + Zn $\rightleftharpoons$ [Mnx-Zn], which is governed by $K_i = \frac{[\text{Mnx}][\text{Zn}]}{[\text{Mnx}\cdot\text{Zn}]}$. As supported by EPR observations, Mn(II) binds to both uninhibited Mnx and Zn-bound Mnx complex [Mnx-Zn], with the corresponding binding rates k^o (known from the experiments without Zn(II)) and k', respectively. Assuming that Zn(II)-bound Mnx, [Mnx-Zn], binds Mn(II) and produces MnO$_2$ very slowly and therefore does not contribute to the initial accumulation of MnO$_2$ product, the initial production of MnO$_2$ is governed only by the fraction of uninhibited [Mnx-Mn] existing in solution. Thus, reducing the binding rate k^o by the ratio [Mnx]/[E$_T$] = 1/(1+[Zn]/K_i), where [E$_T$]=[Mnx]+[Mnx-Zn] is the total concentration of Mnx, the observed binding rate of Mn(II) to Mnx pre-equilibrated with Zn(II), converted to the lag time, is:

$$x_o = \frac{1}{k_{obs}} = \frac{1}{k^0}\left[1 + \frac{[Zn]}{K_i}\right] \tag{2}$$

This equation was used to fit the linear dependence of the lag phase on Zn(II) concentration in Fig. 4A, keeping k^0 fixed (at a value $k^0 = k_{on} * [Mn] + k_{off}$, where k_{on} and k_{off} are known from the lag-phase dependence on Mn(II) concentration in the absence of inhibitor, Fig. S4). For 20, 50, and 100 µM Mn(II), the obtained K_i(Zn) is approximately the same: 1.41±0.14 µM, 1.62±0.09 µM, and 1.65±0.20 µM, respectively. Thus, Zn(II) binds noncompetitively to Mnx, as EPR suggests, with K_i of ~1.5 µM, and the lag time dependence on Zn(II) concentration reflects the rate of Mn(II) binding to uninhibited Mnx whose fraction in solution is governed by K_i(Zn): the lag time slows down with increasing Zn(II), but this effect can be counteracted by increasing the Mn(II) concentration.

Similarly, the observed activation rate constant is simply the rate constant in the absence of an inhibitor, k_{act}^o, reduced by the uninhibited fraction of Mnx existing in equilibrium with [Mnx-Zn]:

$$k_{act} = k_{act}^o * \frac{1}{1+\frac{[Zn]}{K_i}} \qquad (3)$$

Fitting the k_{act} dependence to this equation and fixing k_{act}^o at a known value 0.026 s^{-1} (from Fig. S4B) gives the K_i for Zn(II) ~ 1.5 μM for both Mn(II) concentrations, in close agreement with the value obtained from the lag phase dependence. Thus, both kinetic parameters, the initial binding rate and the activation rate constant, interpreted with the assumption that Zn-bound Mnx produces MnO_2 very slowly, imply that Zn(II) does not compete with Mn(II) for substrate site, binding instead to a separate, inhibitory, site.

3.2.3. Turnover kinetics likewise shows noncompetitive inhibition

Steady-state turnover of Mn(II) also shows a rapid decline with increasing Zn(II) concentration (Fig. S5–S7). When the reciprocals of the steady-state rate were plotted against Zn(II) concentration, as in the form of Dixon plot [73, 74] (Fig. 5), the points fall on straight lines for each Mn(II) concentration and intersect on the x-axis, confirming the noncompetitive nature of Zn(II) inhibition and giving a K_i(Zn) ~ 1.1 μM, in good agreement with the value derived from the lag phase and activation constant dependences.
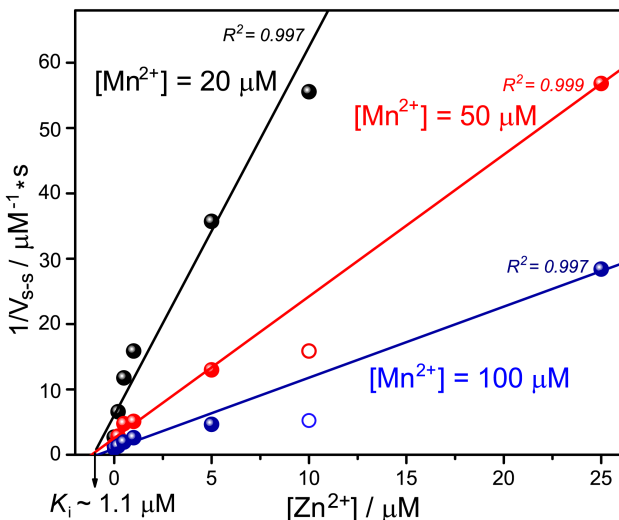
Fig. 5. Inhibition of Mnx turnover rate by Zn(II) during Mnx-catalyzed oxidation of indicated amount of MnSO$_4$ in 10mM HEPES buffer, pH 7.8, plotted as Dixon plot to get K_i(Zn) ~ 1 μM as a common x-axis intersect of linear fits (an assay error in the 10 μM runs likely produced anomalous values (circles), which were excluded from the fits).

Thus, the experiments above all indicate that Zn(II) does not compete with Mn(II) substrate binding sites, but binds to a separate site, hindering Mn(II) binding, enzyme activation step, and inhibiting Mn(II) oxidation.

3.3. Mnx inhibition by Co(II), Ni(II), and Cu(II)

Inhibition of Mn-oxidation activity of Mnx by Co(II), Ni(II), and Cu(II) was also tested, at a single Mn(II) concentration of 50 μM and over a range of inhibiting metals concentrations, to analyze lag, activation, and turnover phases (Fig. S8–S10). (Fe(II) was not included because Mnx is able to oxidize Fe(II) directly, albeit at a lower pH and at a slower rate compared to native Mn(II) substrate [75], thus potentially complicating any additional inhibitory effect on Mn(II) oxidation.) Previous studies with Mn(II)-oxidizing spore extract pointed to the possibility that Co(II) can be oxidized enzymatically by Mn-oxidizing organisms, since Co(III) oxides were found to co-precipitate together with Mn oxides [68]. However, we showed conclusively [69] that Co(II) is not a substrate of Mn-oxidizing factor in *Bacillus* species, but is oxidized indirectly by the enzymatically generated, highly reactive MnO$_2$ nanoparticulates. Indeed, we confirmed

14

here that incubating Co(II) with Mnx for prolonged amount of time does not lead to any visible oxidative reaction, while in the presence of Mn(II), addition of Co(II) modifies the colloidal MnO$_2$ with a broad feature around 600 nm (Fig. S11A), likely due to Co(III) oxides, or Co(III) incorporated within MnO$_2$ structure, as has been reported previously [40, 41, 76, 77]. With 75 μM and 100 μM Co(II), the manganese oxide product precipitated (Fig. S11B). Thus, the upper concentration limit for the Co(II) inhibitor in the Mnx assays was set to 50 μM to avoid interference from oxide precipitation.

The lag time, corresponding to the initial Mn(II) binding, increases linearly as the inhibiting metal concentration increases (Fig. 6A), the slope, which is the reciprocal of K_i (eq. 2), being largest for Cu(II), followed by Zn(II), Ni(II), and Co(II). This corresponds to Irving-Williams order for the relative affinities of a chelator [56, 57]. Treating the Cu-dependence similarly to Zn(II) data (eq. 2), the obtained inhibition constant for Cu(II) is 0.74±0.02 μM. (We note the conditional nature of the K_i value obtained for Cu(II), since with pKa = 8, almost half of Cu(II) species are present as Cu(OH)$^+$ at the experimental pH of 7.8 [78].)
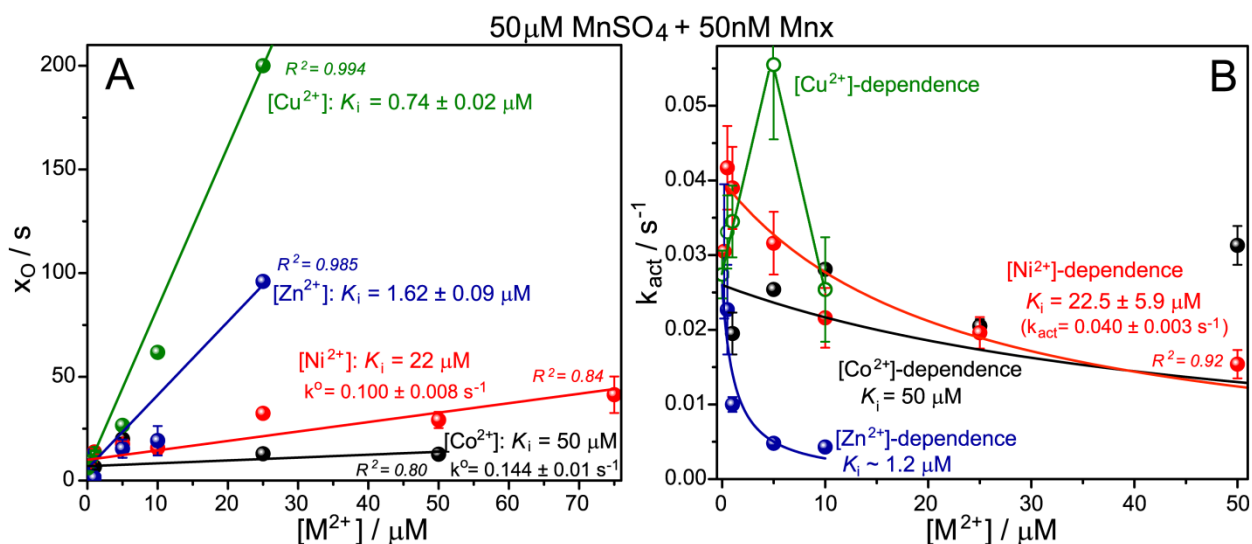

Fig. 6. Inhibition of Mn(II) binding to Mnx (A) and of the subsequent activation step (B) by varying amounts of Co(II), Ni(II), Zn(II), and Cu(II), during oxidation of 50 μM Mn(II) by 50nM Mnx in 10mM HEPES buffer, pH 7.8. (At Cu(II) concentration above 10 μM, the sigmoidal

nature of MnO$_2$ kinetic trace is distorted and cannot be fitted to the activation equation (1), see Fig. S10.)

A similar order is seen for the metal dependences of the activation (Fig. 6B) and turnover (Fig. 7A) phases. A Dixon plot of the turnover rates (Fig. 7B) gives well-behaved extrapolations to the x-axis for Zn(II), Ni(II), and Co(II), giving K_i values of 1.1 µM, 22 µM, and 50 µM, respectively. These values were used to draw the expected lines in the lag-phase dependences in Fig. 6A for the more weakly inhibiting Ni(II) and Co(II), because uncertainties in the lag time prevent an independent fit for K_i for these metals. For the activation rates (Fig. 6B), the Ni(II) data are good enough for an independent fit, which is in good agreement with the Dixon plot value, while the Co(II) data remain uncertain, and the expected curve is drawn with K_i = 50 µM.
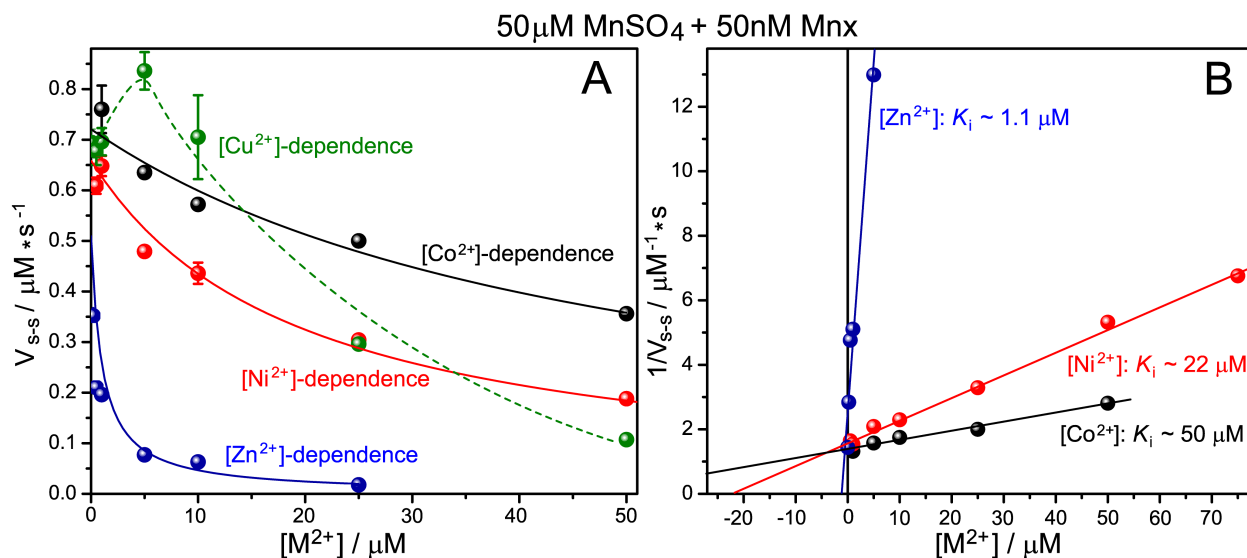
Fig. 7. (A) Inhibition of Mnx turnover rate by four divalent metals during oxidation of 50 µM Mn(II) by 50nM Mnx in 10mM HEPES buffer, pH 7, plotted in (B) as in Dixon form to derive inhibition constants K_i at the x-axis intersect of respective linear fits. For Cu(II)-dependence in (A), the green dashed line was drawn through the last four points to guide the eyes.

For Cu(II), the activation and turnover plots are anomalous (Fig. 6B and 7A). Both reveal acceleration of the rates at low Cu(II), up to 5 µM, followed by strong inhibition. The rise

and fall of k_{act} and V_{s-s} implies that there are two Cu(II) binding sites. The second site is inhibitory, while the first is stimulatory (*see Discussion*).

We considered the possibility that Zn(II) inhibition might be explained by its displacing Cu(II) at the stimulatory site. In that event, addition of Cu(II) to reverse such displacement should diminish Zn(II) inhibition. However, addition of Cu(II) at an activating concentration of 0.5 μM had essentially no effect on the inhibition of Mnx by Zn(II) (Fig. 8). Thus, the inhibitory site is clearly separate from the Cu(II)-activation site.
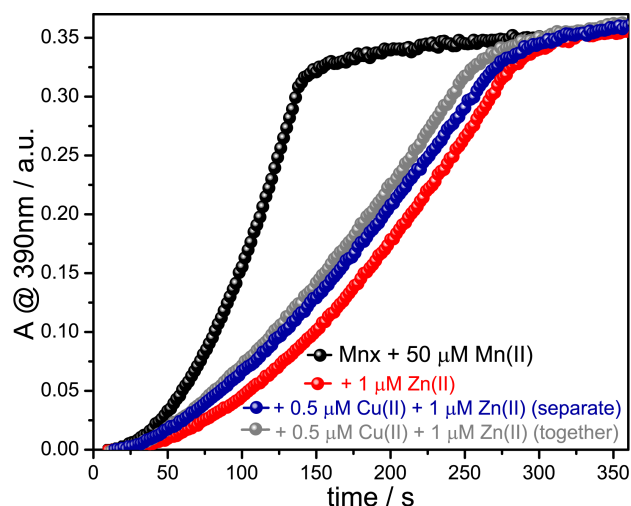
Fig. 8. Progress curves of MnO_2 product formation, taken at 390 nm during oxidation of 50 μM $MnSO_4$ by 50 nM Mnx in 10mM HEPES at pH7.8, in the presence of 1 μM $ZnSO_4$ and 0.5 μM $CuSO_4$, added separately or together, as indicated.

4. DISCUSSION

4.1. Noncompetitive inhibition of Mnx by Zn(II)

Bacterial manganese oxidase Mnx is unique in its ability to catalyze Mn(II) oxidation and mineralization. After Mn(II) binding, the Mnx mechanism (Fig. 1) is triggered by a cascade of activating events: deprotonation of the Mn(II)-bound water that prompts the formation of hydroxide-bridged dinuclear Mn(II) species, and a concomitant Mnx conformation change that "locks" the enzyme in the active form for high selectivity towards its native substrate and fast

electron transfer. Subsequent Mn(II) turnover involves sequential oxidation and formation of dinuclear Mn species, culminating in Mn(IV)-oxo species that nucleate into mineral product.

Zn(II) strongly inhibits the reaction, affecting each stage of the Mnx catalysis: Mn(II) binding, Mnx activation, and turnover. Our kinetic experiments, supported by EPR studies, demonstrate that Zn(II) does not compete with Mn(II) for binding at the substrate site. The inhibition constant for Zn(II), ~1.5 μM, does not vary with Mn(II) concentration, and is consistent with the data at each step of the enzymatic reaction. Analysis of turnover rates with the Dixon plot also confirms the noncompetitive nature of Zn(II) inhibition. What is the inhibition mechanism? We propose an allosteric mechanism, with Zn(II) bind stabilizing Mnx in its inactive form. It thereby prevents the conformation change that otherwise triggers enzyme activation and couples the two Mnx-bound Mn(II) for efficient electron transfer (Fig. 9). Without activation, the turnover of uncoupled Mn(II) species proceed very slowly.
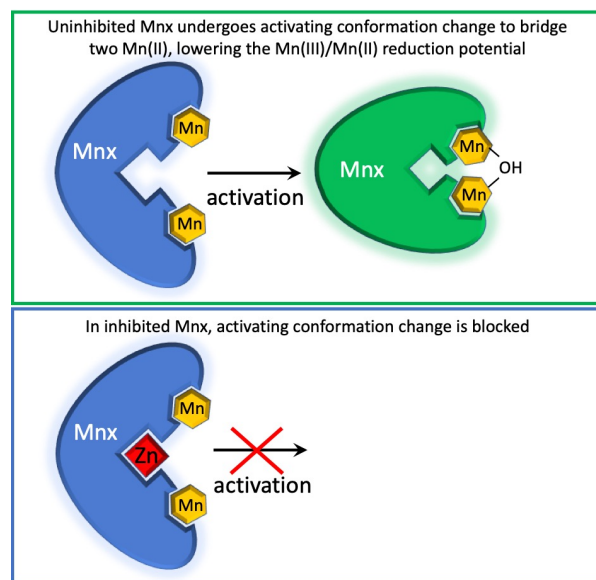
Fig. 9. Proposed mechanism of Zn(II) inhibition of activation step during Mnx-catalyzed Mn(II)-oxidation reaction. The blue protein cartoon depicts Mnx in its inactive form, while the green protein cartoon represents activated Mnx (also green Mnx in the reaction scheme, above); the conformation change results in coupling of two bound Mn(II) ions.

Despite the complexity of steps involved, the observed inhibition can be simply described by accounting for the fraction of "free" Mnx, not bound to Zn(II). The lag phase, representing the initial Mn(II) binding to unactivated enzyme, increases when Zn(II) is bound because the rate of MnO_2 production decreases with less activatable Mnx. Likewise the activation and turnover rates decrease in proportion to the fraction of Zn(II)-bound Mnx. The data are all consistent with a model in which Zn(II) binding at a distinct inhibition site blocks Mnx activation.

Consistent with this model, we observed that the inhibition is lifted when Mnx is pre-activated by first allowing it to turn over a small aliquot of Mn(II), before adding Zn(II) (Fig. S12). The inhibition site becomes inaccessible to Zn(II), presumably because of the conformation change that accompanies activation. This effect can explain the reported observation that Zn(II) prevents Mn oxide formation in a crude solution of a fungal MCO-type Mn oxidase, unless preformed biogenic Mn oxide is present, in which case the Zn(II) inhibition is abolished [40]. The enzyme there may have been activated by the previous round of Mn(II) oxidation, or the preformed oxide may have released sufficient Mn(II) to re-activate the enzyme.

4.2. Mnx inhibition site

In addition to Zn(II), other essential divalent metals Co(II), Ni(II), and Cu(II) inhibit Mnx, with inhibition rate constants all in the micromolar range. The inhibition trend among these metals falls within Irving–Williams series, the pattern that describes competition of the metals for binding to amino acid residues on proteins [56]. The Mnx structure has yet to be determined, but we modeled the possible inhibitory site of Mnx using a MnxG homology model [22] based on the ceruloplasmin structure [79] and the reported structure of a fungal laccase, McoG, from *Aspergillus niger* [80], where adventitious Zn(II) bound near the T1-Cu center was identified. This Zn(II) was found coordinated by His253 and shared a His ligand with the T1-Cu, with a

chloride ion and a water molecule completing the Zn(II) tetrahedral coordination site. When the MnxG and McoG structures were both aligned to ceruloplasmin via the conserved T1-Cu ligands (Fig. 10), the Zn(II) was ~4.6 Å away from the ceruloplasmin Fe(II) substrate site, where Mn(II) is likely bound in Mnx. Mnx-His715 is favorably situated to coordinate Zn(II), and the Mnx-His340, known from previous mutagenesis studies to ligate the T1-Cu [72], could bridge to the Zn(II) site. In the absence of the Mnx atomic-resolution structure, this model is only suggestive, but it provides a basis for probing the inhibitory site in future mutation studies.
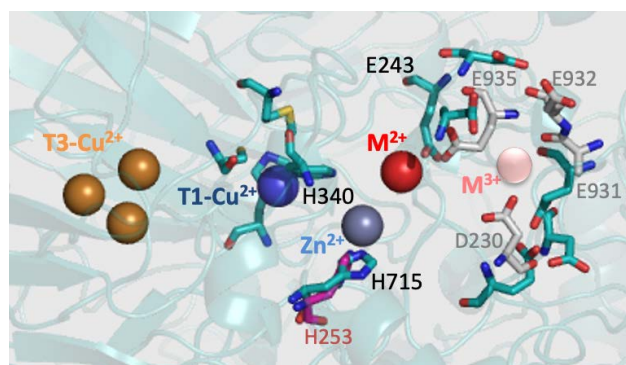
Fig. 10. Structural model for a possible inhibitory site of Mnx, constructed using PyMol [The PyMOL Molecular Graphics System, Version 2.0 Schrödinger, LLC]. The MnxG structural model was predicted by I-TASSER, based on the homology to human ceruloplasmin [22]. It was aligned to the X-ray structure of human ceruloplasmin (PDB:1KCW) [81], to show the trinuclear T2/T3Cu centers (brown spheres), the T1 Cu center (blue) with its conserved ligands, and a possible Mn substrate site, based on the positions of the ceruloplasmin Fe^{2+} substrate (red) and Fe^{3+} product (pink). The suggested inhibitory site is position of the Zn (gray sphere) bound to *Aspergillus niger* laccase McoG (PDB:5LWW) [80], which was also aligned to the ceruloplasmin structure using T1Cu center ligands. In the McoG laccase, the Zn atom is bound to H253, in the location of MnxG His 715, and to one of the T1Cu His ligands, analogous to the MnxG H340. The distance between M^{2+} substrate and Zn(II) is ~ 4.6 Å.

4.3. Effect of Cu(II) on Mn(II) oxidation by Mnx

While Co(II), Ni(II), and Zn(II) follow the Irving–Williams series as Mnx inhibitors, the effect of added Cu(II) is complex. It does follow the series in slowing the rate of Mn binding (lag phase) to the largest extent, but the activation and turnover steps actually *speed up* at low Cu(II), before falling sharply at higher Cu(II). This observation suggests that Cu(II) additionally binds at a separate, enabling site, before binding to the inhibitor site. A similar Cu(II) stimulation

followed by inhibition of Mn-oxidation activity was documented in studies with whole organisms and Mn-oxidizing extracts [82-85]. This observation was used to establish that the enzyme responsible for Mn(II) oxidation in bacterial extracts is a copper-dependent oxidase. The stimulatory effect was attributed to filling of undersaturated Cu sites. However, purified Mnx has a full complement of the four essential MCO Cu(II) centers (T1-Cu plus the trinuclear Cu cluster), consistent with other MCO enzymes.

In addition to the four canonical MCO Cu cofactors, Mnx has an extra T2-type copper on MnxG (as well as three T2-type Cu(II) sites on the MnxEF ring), as quantified in our previous EPR studies [58]. Plus, there are multiple weakly bound Cu sites that can be removed with additional Tris-dialysis treatment [58, 75]. Perhaps, saturation of these sites might account for the stimulatory behavior. We note that the copper detoxification protein CueO from *E. coli* [86, 87], a multicopper oxidase that oxidizes Cu(I) to Cu(II), binds an extra Cu at an internal site next to the T1-Cu and shuttles electrons from the Cu(I) substrate bound at two surface-exposed sites [88, 89]. Perhaps extra Cu sites in Mnx are likewise involved in electron transfer from the Mn(II) substrate.

4.4. Biological function of an inhibitory site in Mnx

Why would manganese-oxidation activity of Mnx be impacted by an inhibitory metal binding site? In manganese-oxidizing *Bacillus* species, it is dormant spores, not metabolically active cells, that possess Mn-oxidizing activity. This activity is often localized in the exosporium, the loose-fitting outermost layer that surrounds some bacterial spores. The Mnx complex takes residence in this outside hydrophobic layer [16] and oxidizes dissolved Mn(II) the spore encounters in the immediate environment, covering the entire spore surface with manganese-oxide crust. The spore can remain dormant for a long period of time, but when it senses specific

nutrients, it initiates the germination process to become again a growing and dividing cell. We observed earlier [90] that once the spores commit to germination, they quickly lose their ability to oxidize Mn(II). Interestingly, in some *Bacillus* spores during the early stages of germination, release of the spores' Zn(II) content represents an initial biochemical event [91, 92]. We propose that the Zn flux reaches the Mnx inhibitory site and shuts off its Mn-oxidizing activity, to keep the Mn(II) pool bioavailable for the growing cell.

Mn(II) is an essential micronutrient for the growth and metabolic activity of bacteria [93, 94]. It serves a protective role against oxidative stress through enzymatic (Mn-superoxide dismutase), and small-molecule (Mn^{2+} ions complexed with low molecular weight species such as phosphate or amino acids) pathways [95]. However, manganese is also a requirement for sporulation and longevity in *Bacillus* species [96-98]. It was shown to protect the spores against ionizing radiation and hydrogen peroxide, perhaps by preventing oxidative damage of enzymes involved in the repair of spore DNA [98, 99]. During the spore formation, Mn^{2+}, together with other metals, mainly Ca^{2+} and Mg^{2+}, and an abundant molecule, pyridine-2,6-dicarboxylic acid (dipicolinic acid), accumulates in the highly dehydrated spore core where bacterial DNA is protected [97, 100-103]. Our previous studies with whole spores indicated that Mnx is expressed during the mid-to-late stages of sporulation process [82], stages that also see core dehydration and mineralization. Thus, another possible role for Zn(II)-inhibition could be to keep Mnx inactive during spore assembly by the mother cell, while the enzyme is being expressed and transported to the exosporium. Zn(II) binding to Mnx would prevent intracellular MnO_2 formation, allowing for Mn(II) to be taken up by the spore core. Once the mature spore is released from the mother cell, Zn(II) would dissociate from Mnx in the exosporium, turning on Mn(II) oxidation activity.

Another possibility is that the Zn(II)-inhibition site can act as an on/off switch to regulate manganese access in symbiotic associations of Mn-oxidizing bacteria with Mn-reducing bacteria or other hosts. We note that manganese-oxidizing bacteria were found living in a symbiotic relationship with sponges, where the bacteria were proposed to maintain the physiological Mn concentrations in their hosts (described specifically for *S. domuncula* sponges) [104]. The sponges might regulate the bacterial Mnx enzyme through their own Zn efflux system, to turn off Mn-oxidation activity and access the bioavailable Mn when needed.

5. CONCLUSIONS

Mnx is unique among multicopper oxidases in efficiently catalyzing the two-electron oxidation and biomineralization of manganese. It brings the high redox potential chemistry of manganese to a more accessible range through a conformational change that allows formation of polynuclear manganese centers in successive oxidation states at the enzyme active sites. We found that Zn(II) and other transition metals (Co(II), Ni(II), and Cu(II)) inhibit the reaction, in the Irving-Williams order, through a non-competitive mechanism. EPR showed that adding Zn(II) or other divalent metals to Mnx does not perturb the native bound Mn(II) signals, either mono- or dinuclear, indicating that the substrate sites are specific for Mn(II). Kinetic measurements of Mnx oxidation confirm that these inhibiting transition metals do not compete with Mn(II) for the substrate sites on Mnx, but bind at a separate inhibitory site. We propose that filling this site prevents the enzyme conformational change that enables Mn(II) oxidation. Interestingly, addition of Cu(II) initially enhances the activation and turnover steps of Mn(II) oxidation, before subsequently inhibiting the enzyme. We attribute this activation to filling of extra Cu sites that may play an electron-transfer role in catalysis.

Inactivation of Mnx by divalent metals, and also the stimulatory effect of sub-micromolar concentrations of Cu(II) are also observed for whole *Bacillus* spores, and can be attributed to Mnx being a surface-exposed enzyme in the exosporium. However, nothing is known about the molecular context of Mnx in the complex exosporium layer of the spores. There may be other Zn or Cu binding proteins in the vicinity of Mnx, which could modulate its function and its possible communication with the spore interior or with neighboring cells. Future work will be directed at elucidating this higher level of biological complexity in manganese biomineralization.

ABBREVIATIONS

CW EPR: continuous-wave electron paramagnetic resonance
CueO: copper-detoxification multicopper oxidase from *E. coli*
Fet3p: ferroxidase, a multicopper oxidase found in *Saccharomyces cerevisiae*
EPR: electron paramagnetic resonance
HEPES: 4-(2-hydroxyethyl)-1-piperazineethanesulfonic acid
MCO: multicopper oxidase
McoG: fungal laccase from *Aspergillus niger*
MCR-ALS: Multivariate Curve Resolution–Alternating Least-Squares algorithm
Mnx: manganese oxidase complex Mnx from *Bacillus* sp. PL-12
T1-Cu: type 1 copper center of multicopper oxidases

ACKNOWLEDGMENT

Appendix A. Supplementary data

UV-vis absorption band of enzymatic MnO_2 product obtained under different conditions; collections of the fitted time courses of the MCR-ALS-resolved enzymatic component of Mnx-catalyzed Mn(II) oxidation in the presence of different metals, to extract parameters used to plot [$MnSO_4$]-dependence in Fig. S4, and metal inhibitor-dependences in Fig. 4–7 in the main text; dependence of the final MnO_2 band and MnO_2 time courses on Co(II) concentration; detailed description and results of the successive addition experiment in the presence of Zn(II).

REFERENCES

[1] Learman, D. R., Voelker, B. M., Vazquez-Rodriguez, A. I., and Hansel, C. M. (2011) Formation of manganese oxides by bacterially generated superoxide, *Nat. Geosci. 4*, 95–98.

[2] Learman, D. R., Wankel, S. D., Webb, S. M., Martinez, N., Madden, A. S., and Hansel, C. M. (2011) Coupled biotic-abiotic Mn(II) oxidation pathway mediates the formation and structural evolution of biogenic Mn oxides, *Geochim. Cosmochim. Acta 75*, 6048–6063.

[3] Hansel, C. M., Zeiner, C. A., Santelli, C. M., and Webb, S. M. (2012) Mn(II) oxidation by an *Ascomycete* fungus is linked to superoxide production during asexual reproduction, *Proc. Natl. Acad. Sci. U.S.A. 109*, 12621–12625.

[4] Learman, D. R., Voelker, B. M., Madden, A. S., and Hansel, C. M. (2013) Constraints on superoxide mediated formation of manganese oxides, *Front. Microbiol. 4*, 262.

[5] Andeer, P. F., Learman, D. R., McIlvin, M., Dunn, J. A., and Hansel, C. M. (2015) Extracellular haem peroxidases mediate Mn(II) oxidation in a marine *Roseobacter* bacterium via superoxide production, *Environ. Microbiol. 17*, 3925–3936.

[6] Tebo, B. M., Ghiorse, W. C., van Waasbergen, L. G., Siering, P. L., and Caspi, R. (1997) Bacterially-mediated mineral formation: Insights into manganese(II) oxidation from molecular genetic and biochemical studies, in *Geomicrobiology: interactions between microbes and minerals* (Banfield, J. F., and Nealson, K. H., Eds.), pp 225–266, Mineralogical Society of America, Washington, D.C.

[7] Tebo, B. M., Johnson, H. A., McCarthy, J. K., and Templeton, A. S. (2005) Geomicrobiology of manganese(II) oxidation, *Trends Microbiol. 13*, 421–428.

[8] Geszvain, K., Butterfield, C. N., Davis, R. E., Madison, A. S., Lee, S.-W., Parker, D. L., Soldatova, A. V., Spiro, T. G., Luther III, G. W., and Tebo, B. M. (2012) The molecular biogeochemistry of manganese(II) oxidation, *Biochem. Soc. Trans. 40*, 1244–1248.

[9] Anderson, C. R., Johnson, H. A., Caputo, N., Davis, R. E., Torpey, J. W., and Tebo, B. M. (2009) Mn(II) oxidation is catalyzed by heme peroxidases in *"Aurantimonas manganoxydans"* strain SI85-9A1 and *Erythrobacter* sp. strain SD-21, *Appl. Environ. Microbiol. 75*, 4130–4138.

[10] Geszvain, K., Smesrud, L., and Tebo, B. M. (2016) Identification of a third Mn(II) oxidase enzyme in *Pseudomonas putida* GB-1, *Appl. Environ. Microbiol. 82*, 3774–3782.

[11] Zámocký, M., Hofbauer, S., Schaffner, I., Gasselhuber, B., Nicolussi, A., Soudi, M., Pirker, K. F., Furtmüller, P. G., and Obinger, C. (2015) Independent evolution of four heme peroxidase superfamilies, *Arch. Biochem. Biophys. 574*, 108–119.

[12] Corstjens, P. L. A. M., de Vrind, J. P. M., Goosen, T., and de Vrind-de Jong, E. W. (1997) Identification and molecular analysis of the Leptothrix discophora SS-1 mofA gene a gene putatively encoding a manganese-oxidizing protein with copper domains, *Geomicrobiol. J. 14*, 91–108.

[13] Geszvain, K., McCarthy, J. K., and Tebo, B. M. (2013) Elimination of manganese(II,III) oxidation in *Pseudomonas putida* GB-1 by a double knockout of two putative multicopper oxidase genes, *Appl. Environ. Microbiol. 79*, 357–366.

[14] Brouwers, G.-J., Vijgenboom, E., Corstjens, P. L. A. M., de Vrind, J. P. M., and de Vrind-de Jong, E. W. (2000) Bacterial Mn^{2+} oxidizing systems and multicopper oxidases: an overview of mechanisms and functions, *Geomicrobiol. J. 17*, 1–24.

[15] Dick, G. J., Torpey, J. W., Beveridge, T. J., and Tebo, B. M. (2008) Direct identification of a bacterial manganese(II) oxidase, the multicopper oxidase MnxG, from spores of several different marine *Bacillus* species, *Appl. Environ. Microbiol. 74*, 1527–1534.

[16] Francis, C. A., Casciotti, K. L., and Tebo, B. M. (2002) Localization of Mn(II)-oxidizing activity and the putative multicopper oxidase, MnxG, to the exosporium of the marine *Bacillus* sp. strain SG-1, *Arch. Microbiol. 178*, 450–456.

[17] Ridge, J. P., Lin, M., Larsen, E. I., Fegan, M., McEwan, A. G., and Sly, L. I. (2007) A multicopper oxidase is essential for manganese oxidation and laccase-like activity in *Pedomicrobium* sp. ACM 3067, *Environ. Microbiol. 9*, 944–953.

[18] Solomon, E. I., Sundaram, U. M., and Machonkin, T. E. (1996) Multicopper oxidases and oxygenases, *Chem. Rev. 96*, 2563–2605.

[19] Kosman, D. J. (2010) Multicopper oxidases: a workshop on copper coordination chemistry, electron transfer, and metallophysiology, *J. Biol. Inorg. Chem. 15*, 15–28.

[20] Butterfield, C. N., Soldatova, A. V., Lee, S.-W., Spiro, T. G., and Tebo, B. M. (2013) Mn(II,III) oxidation and MnO_2 mineralization by an expressed bacterial multicopper oxidase, *Proc. Natl. Acad. Sci. U.S.A. 110*, 11731–11735.

[21] Francis, C. A., and Tebo, B. M. (2002) Enzymatic manganese(II) oxidation by metabolically dormant spores of diverse *Bacillus* species, *Appl. Environ. Microbiol. 68*, 874–880.

[22] Romano, C. A., Zhou, M., Song, Y., Wysocki, V. H., Dohnalkova, A. C., Kovarik, L., Paša-Tolić, L., and Tebo, B. M. (2017) Biogenic manganese oxide nanoparticle formation by a multimeric multicopper oxidase Mnx, *Nat. Commun. 8*, 746.

[23] Soldatova, A. V., Tao, L., Romano, C., Stich, T. A., Casey, W. H., Britt, R. D., Tebo, B. M., and Spiro, T. G. (2017) Mn(II) oxidation by the multicopper oxidase complex Mnx: A binuclear activation mechanism, *J. Am. Chem. Soc. 139*, 11369−11380.

[24] Soldatova, A. V., Romano, C., Tao, L., Stich, T. A., Casey, W. H., Britt, R. D., Tebo, B. M., and Spiro, T. G. (2017) Mn(II) oxidation by the multicopper oxidase complex Mnx: A coordinated two-stage MnII/MnIII and MnIII/MnIV mechanism, *J. Am. Chem. Soc. 139*, 11381−11391.

[25] Santelli, C. M., Webb, S. M., Dohnalkova, A. C., and Hansel, C. M. (2011) Diversity of Mn oxides produced by Mn(II)-oxidizing fungi, *Geochim. Cosmochim. Acta 75*, 2762–2776.

[26] Villalobos, M., Toner, B., Bargar, J., and Sposito, G. (2003) Characterization of the manganese oxide produced by *Pseudomonas putida* strain MnB1, *Geochim. Cosmochim. Acta 67*, 2649–2662.

[27] Miyata, N., Tani, Y., Iwahori, K., and Soma, M. (2004) Enzymatic formation of manganese oxides by an *Acremonium*-like hyphomycete fungus, strain KR21-2, *FEMS Microbiol. Ecol. 47*, 101–109.

[28] Webb, S. M., Tebo, B. M., and Bargar, J. R. (2005) Structural characterization of biogenic manganese oxides produced in sea water by the marine *Bacillus* sp. strain SG-1, *Am. Mineral. 90*, 1342–1357.

[29] Zhu, M., Ginder-Vogel, M., Parikh, S. J., Feng, X.-H., and Sparks, D. L. (2010) Cation effects on the layer structure of biogenic Mn-oxides, *Environ. Sci. Technol. 44*, 4465–4471.

[30] Saratovsky, I., Wightman, P. G., Pasten, P. A., Gaillard, J.-F., and Poeppelmeier, K. R. (2006) Manganese oxides: Parallels between abiotic and biotic structures, *J. Am. Chem. Soc. 128*, 11188–11198.

[31] Feng, X. H., Zhu, M., Ginder-Vogel, M., Ni, C., Parikh, S. J., and Sparks, D. L. (2010) Formation of nano-crystalline todorokite from biogenic Mn oxides, *Geochim. Cosmochim. Acta 74*, 3232–3245.

[32] Spiro, T. G., Bargar, J. R., Sposito, G., and Tebo, B. M. (2010) Bacteriogenic manganese oxides, *Acc. Chem. Res. 43*, 2–9.

[33] Tebo, B. M., Bargar, J. R., Clement, B., Dick, G., Murray, K. J., Parker, D., Verity, R., and Webb, S. M. (2004) Biogenic manganese oxides: Properties and mechanisms of formation, *Annu. Rev. Earth Planet. Sci. 32*, 287–328.

[34] Remucal, C. K., and Ginder-Vogel, M. (2014) A critical review of the reactivity of manganese oxides with organic contaminants, *Environ. Sci. Process. Impacts 16*, 1247–1266.

[35] Sunda, W. G., and Kieber, D. J. (1994) Oxidation of humic substances by manganese oxides yields low-molecular-weight organic substrates, *Nature 367*, 62–64.

[36] Lafferty, B. J., Ginder-Vogel, M., and Sparks, D. L. (2010) Arsenite oxidation by a poorly crystalline manganese-oxide 1. Stirred-flow experiments, *Environ. Sci. Technol. 44*, 8460–8466.

[37] Schacht, L., and Ginder-Vogel, M. (2018) Arsenite depletion by manganese oxides: A case study on the limitations of observed first order rate constants, *Soil Syst. 2*, 39.

[38] Stone, A. T., and Morgan, J. J. (1984) Reduction and dissolution of manganese(III) and manganese(IV) oxides by organics: 2. Survey of the reactivity of organics, *Environ. Sci. Technol. 18*, 617–624.

[39] Chang, J., Tani, Y., Naitou, H., Miyata, N., Tojo, F., and Seyama, H. (2014) Zn(II) sequestration by fungal biogenic manganese oxide through enzymatic and abiotic processes, *Chem. Geol. 383*, 155–163.

[40] Chang, J., Yukinori Tani, Y., Naitou, H., Miyata, N., Seyama, H., and Tanaka, K. (2013) Cobalt(II) sequestration on fungal biogenic manganese oxide enhanced by manganese(II) oxidase activity, *Appl. Geochem. 37*, 170–178.

[41] Yu, Q. Q., Sasaki, K., Tanaka, K., Ohnuki, T., and Hirajima, T. (2012) Structural factors of biogenic birnessite produced by fungus *Paraconiothyrium* sp WL-2 strain affecting sorption of Co^{2+}, *Chem. Geol. 310*, 106–113.

[42] Villalobos, M., Bargar, J., and Sposito, G. (2005) Mechanisms of Pb(II) sorption on a biogenic manganese oxide, *Environ. Sci. Technol. 39*, 569–576.

[43] Simonov, A. N., Hocking, R. K., Tao, L., Gengenbach, T., Williams, T., Fang, X.-Y., King, H. J., Bonke, S. A., Hoogeveen, D. A., Romano, C. A., Tebo, B. M., Martin, L. L., Casey, W. H., and Spiccia, L. (2017) Tunable biogenic manganese oxides, *Chem. Eur. J. 23*, 13482–13492.

[44] Webb, S. M., Tebo, B. M., and Bargar, J. R. (2005) Structural influences of sodium and calcium ions on the biogenic manganese oxides produced by the marine *Bacillus* sp., strain SG-1, *Geomicrobiol. J. 22*, 181–193.

[45] Webb, S. M., Fuller, C. C., Tebo, B. M., and Bargar, J. R. (2006) Determination of uranyl incorporation into biogenic manganese oxides using x-ray absorption spectroscopy and scattering, *Environ. Sci. Technol. 40*, 771–777.

[46] Tang, Y., Webb, S. M., Estes, E. R., and Hansel, C. M. (2014) Chromium(iii) oxidation by biogenic manganese oxides with varying structural ripening, *Environ. Sci. Process. Impact 16*, 2127−2136.

[47] Toner, B., Manceau, A., Webb, S. M., and Sposito, G. (2006) Zinc sorption to biogenic hexagonal-birnessite particles within a hydrated bacterial biofilm, *Geochim. Cosmochim. Acta 70*, 27–43.

[48] Liu, W., Sutton, N. B., Rijnaarts, H. H. M., and Langenhoff, A. A. M. (2016) Pharmaceutical removal from water with iron- or manganese-based technologies: A review, *Crit. Rev. Environ. Sci. Technol. 46*, 1584–1621.

[49] Matsushita, S., Komizo, D., Cao, L. T. T., Aoi, Y., Kindaichi, T., Ozaki, N., Imachi, H., and Ohashi, A. (2018) Production of biogenic manganese oxides coupled with methane oxidation in a bioreactor for removing metals from wastewater, *Water Res. 130*, 224–233.

[50] Hennebel, T., De Gusseme, B., Boon, N., and Verstraete, W. (2009) Biogenic metals in advanced water treatment, *Trends Biotechnol. 27*, 90–98.

[51] Tani, Y., Miyata, N., Ohashi, M., Ohnuki, T., Seyama, H., Iwahori, K., and Soma, M. (2004) Interaction of inorganic arsenic with biogenic manganese oxide produced by a Mn-oxidizing fungus, strain KR21-2, *Environ. Sci. Technol. 38*, 6618–6624.

[52] Therdkiattikul, N., Ratpukdi, T., Kidkhunthod, P., Chanlek, N., and Siripattanakul-Ratpukdi, S. (2020) Manganese-contaminated groundwater treatment by novel bacterial isolates: kinetic study and mechanism analysis using synchrotron-based techniques, *Sci. Reports 10*, 13391.

[53] Duckworth, O. W., Rivera, N. A., Gardner, T. G., Andrews, M. Y., Santelli, C. M., and Polizzotto, M. L. (2017) Morphology, strucutre, and metal binding mechanisms of biogenic manganese oxides in a superfund site treatment system, *Environ. Sci. Process. Impact 19*, 50–58.

[54] Furgal, K. M., Meyer, R. L., and Bester, K. (2015) Removing selected steroid hormones, biocides and pharmaceuticals from water by means of biogenic manganese oxide nanoparticles *in situ* at ppb levels, *Chemosphere 136*, 321–326.

[55] Yu, Q., Sasaki, K., Tanaka, K., Ohnuki, T., and Hirajima, T. (2013) Zinc sorption during bio-oxidation and precipitation of manganese modifies the layer stacking of biogenic birnessite, *Geomicrobiol. J. 30*, 829–839.

[56] Irving, H., and Williams, R. J. P. (1948) Order of stability of metal complexes, *Nature 162*, 746–747.

[57] Martin, R. B. (1987) A stability ruler for metal ion complexes, *J. Chem. Educ. 64*, 402.

[58] Tao, L., Stich, T. A., Liou, S.-H., Soldatova, A. V., Delgadillo, D. A., Romano, C. A., Spiro, T. G., Goodin, D. B., Tebo, B. M., Casey, W. H., and Britt, R. D. (2017) Copper binding sites in the manganese-oxidizing Mnx protein complex investigated by Electron Paramagnetic Resonance spectroscopy, *J. Am. Chem. Soc. 139*, 8868–8877.

[59] Tauler, R., Smilde, A., and Kowalski, B. (1995) Selectivity, local rank, three-way data analysis and ambiguity in multivariate curve resolution, *J. Chemometrics 9*, 31–58.

[60] Jaumot, J., Gargallo, R., de Juan, A., and Tauler, R. (2005) A graphical user-friendly interface for MCR–ALS: a new tool for multivariate curve resolution in MATLAB, *Chemometr. Intell. Lab. 76*, 101–110.

[61] Jaumot, J., de Juan, A., and Tauler, R. (2015) MCR-ALS GUI 2.0: New features and applications, *Chemometr. Intell. Lab. 140*, 1–12.

[62] Soldatova, A. V., Balakrishnan, G., Oyerinde, O. F., Romano, C. A., Tebo, B. M., and Spiro, T. G. (2019) Biogenic and synthetic MnO_2 nanoparticles: Size and growth probed with absorption and Raman spectroscopies and dynamic light scattering, *Environ. Sci. Technol. 53*, 4185–4197.

[63] Frieden, C. (1970) Kinetic aspects of regulation of metabolic processes: The hysteretic enzyme concept, *J. Biol. Chem. 245*, 5788–5799.

[64] Adams, L. F., and Ghiorse, W. C. (1987) Characterization of extracellular Mn^{2+}-oxidizing activity and isolation of an Mn^{2+}-oxidizing protein from *Leptothrix discophora* SS-1, *J. Bacteriology 169*, 1279–1285.

[65] Murray, K. J., Mozafarzadeh, M. L., and Tebo, B. M. (2005) Cr(III) oxidation and Cr toxicity in cultures of the manganese(II)-oxidizing *Pseudomonas putida* strain GB-1, *Geomicrobiol. J. 22*, 151–159.

[66] Murray, K. J., and Tebo, B. M. (2007) Cr(III) is indirectly oxidized by the Mn(II)-oxidizing bacterium *Bacillus* sp. strain SG-1, *Environ. Sci. Technol. 41*, 528–533.

[67] Chinni, S., Anderson, C. R., Ulrich, K.-U., Giammar, D. E., and Tebo, B. M. (2008) Indirect UO_2 oxidation by Mn(II)-oxidizing spores of *Bacillus* sp. strain SG-1 and the effect of U and Mn concentrations, *Environ. Sci. Technol. 42*, 8709–8714.

[68] Lee, Y., and Tebo, B. M. (1994) Cobalt(II) oxidation by the marine manganese(II)-oxidizing *Bacillus* sp. strain SG-1, *Appl. Environ. Microbiol. 60*, 2949−2957.

[69] Murray, K. J., Webb, S. M., Bargar, J. R., and Tebo, B. M. (2007) Indirect oxidation of Co(II) in the presence of the marine Mn(II)-oxidizing bacterium Bacillus sp. strain SG-1, *Appl. Environ. Microbiol. 73*, 6905–6909.

[70] McKee, D. J., and Frieden, E. (1971) Binding of transition metal ions by ceruloplasmin (ferroxidase), *Biochemistry 10*, 3880–3883.

[71] Quintanar, L., Gebhard, M., Wang, T. P., Kosman, D. J., and Solomon, E. I. (2004) Ferrous binding to the multicopper oxidases *Saccharomyces cerevisiae* Fet3p and human ceruloplasmin: contributions to ferroxidase activity, *J. Am. Chem. Soc. 126*, 6579–6589.

[72] Tao, L., Stich, T. A., Butterfield, C. N., Romano, C., Spiro, T. G., Tebo, B. M., Casey, W. H., and Britt, R. D. (2015) Mn(II) binding and subsequent oxidation by the multicopper oxidase MnxG investigated by electron paramagnetic resonance spectroscopy, *J. Am. Chem. Soc. 137*, 10563–10575.

[73] Dixon, M. (1953) The determination of enzyme inhibitor constants, *Biochem. J. 55*, 170–171.

[74] Butterworth, P. J. (1972) The use of dixon plots to study enzyme inhibition, *Biochim. Biophys. Acta 289*, 251–253.

[75] Butterfield, C. N., and Tebo, B. M. (2017) Substrate specificity and copper loading of the manganese-oxidizing multicopper oxidase Mnx from *Bacillus* sp. PL-12, *Metallomics 9*, 183–191.

[76] Simanova, A. A., and Peña, J. (2015) Time-resolved investigation of cobalt oxidation by Mn(III)-rich δ-MnO_2 using quick X-ray absorption spectroscopy, *Environ. Sci. Technol. 49*, 10867−10876.

[77] Tanaka, K., Yu, Q., Sasaki, K., and Ohnuki, T. (2013) Cobalt(II) oxidation by biogenic Mn oxide produced by *Pseudomonas* sp. strain NGY-1, *Geomicrobiol. J. 30*, 874–885.

[78] Jackson, V. E., Felmy, A. R., and Dixon, D. A. (2015) Prediction of the pKa's of aqueous metal ion +2 complexes, *J. Phys. Chem. A 119*, 2926–2939.

[79] Bento, I., Peixoto, C., Zaitsev, V. N., and Lindley, P. F. (2007) Ceruloplasmin revisited: structural and functional roles of various metal cation-binding sites, *Acta Crystallogr. D 63*, 240–248.

[80] Ferraroni, M., Westphal, A., Borsari, M., Tamayo-Ramos, J., Briganti, F., Graaff, L., and Berkel, W. (2017) Structure and function of *Aspergillus niger* laccase McoG, *Biocatalysis 3*, 1–21.

[81] Zaitseva, I., Zaitsev, V., Card, G., Moshkov, K., Bax, B., Ralph, A., and Lindley, P. F. (1996) The X-ray structure of human serum ceruloplasmin at 3.1 Å: nature of the copper centres, *JBIC 1*, 15–23.

[82] van Waasbergen, L. G., Hildebrand, M., and Tebo, B. M. (1996) Identification and characterization of a gene cluster involved in manganese oxidation by spores of the marine Bacillus sp. strain SG-1, *J. Bacteriology 178*, 3517–3530.

[83] Brouwers, G.-J., de Vrind, J. P. M., Corstjens, P. L. A. M., Cornelis, P., Baysse, C., and de Vrind-de Jong, E. W. (1999) CumA, a gene encoding a multicopper oxidase, is involved in Mn^{2+}-oxidation in *Pseudomonas putida* GB-1, *Appl. Environ. Microbiol. 65*, 1762–1768.

[84] Brouwers, G. J., Corstjens, P. L. A. M., de Vrind, J. P. M., Verkamman, A., de Kuyper, M., and de Vrind-de Jong, E. W. (2000) Stimulation of Mn^{2+} oxidation in *Leptothrix discophora* SS-1 by Cu^{2+} and sequence analysis of the region flanking the gene encoding putative multicopper oxidase MofA, *Geomicrobiol. J. 17*, 25–33.

[85] Zhang, J., Lion, L. W., Nealson, Y. M., Shuler, M. L., and Ghiorse, W. C. (2002) Kinetics of Mn(II) oxidation by *Leptothrix discophora* SS1, *Geochim. Cosmochim. Acta 65*, 773–781.

[86] Grass, G., and Rensing, C. (2001) CueO is a multi-copper oxidase that confers copper tolerance in *Escherichia coli*, *Biochem. Biophys. Res. Commun. 286*, 902–908.

[87] Singh, S. K., Grass, G., Rensing, C., and Montfort, W. R. (2004) Cuprous oxidase activity of CueO from *Escherichia coli*, *J. Bacteriol. 186*, 7815–7817.

[88] Djoko, K. Y., Chong, L. X., Wedd, A. G., and Xiao, Z. (2010) Reaction mechanisms of the multicopper oxidase CueO from *Escherichia coli* support Its functional role as a cuprous oxidase, *J. Am. Chem. Soc. 132*, 2005–2015.

[89] Cortes, L., Wedd, A. G., and Xiao, Z. (2015) The functional roles of the three copper sites associated with the methionine-rich insert in the multicopper oxidase CueO from *E. coli*, *Metallomics 7*, 776–785.

[90] Tebo, B. M. personal observation.

[91] Johnstone, K., Stewart, G. S., Scott, I. R., and Ellar, D. J. (1982) Zinc release and the sequence of biochemical events during triggering of *Bacillus megaterium* KM spore germination, *Biochem. J. 208*, 407–411.

[92] He, L. M., and Tebo, B. M. (1998) Surface charge properties of and Cu(II) adsorption by spores of the marine *Bacillus* sp. strain SG-1, *Appl. Environ. Microbiol. 64*, 1123–1129.

[93] Ehrlich, H. L. (2002) *Geomicrobiology*, Marcel Dekker, New York, NY, USA.

[94] Jakubovics, N. S., and Jenkinson, H. F. (2001) Out of the iron age: new insights into the critical role of manganese homeostasis in bacteria, *Microbiology 147*, 1709–1718.

[95] Sharma, A., Gaidamakova, E. K., Grichenko, O., Matrosova, V. Y., Hoeke, V., Klimenkova, P., Conze, I. H., Volpe, R. P., Tkavc, R., Gostinčar, C., Gunde-Cimerman, N.,

DiRuggiero, J., Shuryak, I., Ozarowski, A., Hoffman, B. M., and Daly, M. J. (2017) Across the tree of life, radiation resistance is governed by antioxidant Mn^{2+}, gauged by paramagnetic resonance, *Proc. Natl. Acad. Sci. U.S.A. 114*, E9253–E9260.

[96] Vasantha, N., and Freese, E. (1979) The role of manganese in growth and sporulation of *Bacillus subtilis*, *J. Gen. Microbiol. 112*, 329–336.

[97] Kolodziej, B. J., and Slepecky, R. A. (1964) Trace metal requirements for sporulation of *Bacillus megaterium*, *J. bacteriol. 88*, 821–830.

[98] Granger, A. C., Gaidamakova, E. K., Matrosova, V. Y., Daly, M. J., and Setlow, P. (2011) Effects of manganese and iron levels on *Bacillus subtilis* spore resistance and effects of Mn^{2+}, other divalent cations, orthophosphate, and dipicolinic acid on protein resistance to ionizing radiation, *Appl. Environ. Microbiol. 77*, 32–40.

[99] Ghosh, S., Ramirez-Peralta, A., Gaidamakova, E., Zhang, P., Li, Y.-Q., Daly, M. J., and Setlow, P. (2011) Effects of Mn levels on resistance of *Bacillus megaterium* spores to heat, radiation and hydorgen peroxide, *J. Appl. Microbiol. 111*, 663–670.

[100] Lundgren, D. G., and Cooney, J. J. (1962) Chemical analyses of asporogenic mutants of *Bacillus cereus*, *J. bacteriol. 83*, 1287–1293.

[101] Levinson, H. S., and Hyatt, M. T. (1964) Effect of sporulation medium on heat resistance, chemical composition, and germination of *Bacillus megaterium* spores, *J. bacteriol. 87*, 876–886.

[102] Leggett, M. J., McDonnell, G., Denyer, S. P., Setlow, P., and Maillard, J. Y. (2012) Bacterial spore structures and their protective role in biocide resistance, *J. Appl. Microbiol. 113*, 485–498.

[103] Bressuire-Isoard, C., Broussolle, V., and Carlin, F. (2018) Sporulation environment influences spore properties in *Bacillus*: evidence and insights on underlying molecular and physiological mechanisms, *FEMS Microbiol. Rev. 42*, 614–626.

[104] Wang, X., Wiens, M., Divekar, M., Grebenjuk, V. A., Schröder, H. C., Batel, R., and Müller, W. E. (2011) Isolation and characterization of a Mn(II)-oxidizing *Bacillus* strain from the demosponge *Suberites domuncula*, *Mar. Drugs 9*, 1−28.